Atmospheric and oceanic excitation of decadal-scale Earth orientation variations

Richard S. Gross, Ichiro Fukumori, and Dimitris Menemenlis
Jet Propulsion Laboratory, California Institute of Technology, Pasadena, California, USA

Received 6 December 2004; revised 12 May 2005; accepted 9 June 2005; published 3 September 2005.

[1] The contribution of atmospheric wind and surface pressure and oceanic current and bottom pressure variations during 1949–2002 to exciting changes in the Earth's orientation on decadal timescales is investigated using an atmospheric angular momentum series computed from the National Centers for Environmental Prediction/National Center for Atmospheric Research (NCEP/NCAR) reanalysis project and an oceanic angular momentum series computed from a near-global ocean model that was forced by surface fluxes from the NCEP/NCAR reanalysis project. Not surprisingly, since decadal-scale variations in the length of day are caused mainly by interactions between the mantle and core, the effect of the atmosphere and oceans is found to be only about 14% of that observed. More surprisingly, it is found that the effect of atmospheric and oceanic processes on decadal-scale changes in polar motion is also only about 20% (x component) and 38% (y component) of that observed. Therefore redistribution of mass within the atmosphere and oceans does not appear to be the main cause of the Markowitz wobble. It is also found that on timescales between 10 days and 4 years the atmospheric and oceanic angular momentum series used here have very little skill in explaining Earth orientation variations before the mid to late 1970s. This is attributed to errors in both the Earth orientation observations prior to 1976 when measurements from the accurate space-geodetic techniques became available and to errors in the modeled atmospheric fields prior to 1979 when the satellite era of global weather observing systems began.

Citation: Gross, R. S., I. Fukumori, and D. Menemenlis (2005), Atmospheric and oceanic excitation of decadal-scale Earth orientation variations, *J. Geophys. Res.*, *110*, B09405, doi:10.1029/2004JB003565.

1. Introduction

[2] The Earth's orientation, encompassing both the rate of rotation, or equivalently, the length of the day, as well as the position of the rotation pole with respect to the Earth's crust and mantle, changes on all observable timescales, from subdaily to decadal and longer. The wide range of timescales on which the Earth's orientation changes reflects the wide range of processes affecting it, from external tidal forces, to surficial processes involving the atmosphere, oceans, and hydrosphere, to internal processes acting both at the core-mantle boundary as well as within the solid Earth itself. Tidal effects are the main cause of subdaily Earth orientation variations [*Chao et al.*, 1996] and have a major influence on the length of day at longer periods [*Yoder et al.*, 1981; *Defraigne and Smits*, 1999], but have only a minor influence on polar motion at longer periods [*Gross et al.*, 1996, 1997]. Changes in the strength and direction of atmospheric winds are the main cause of nontidal length-of-day variations on timescales of a few days to a few years [e.g., *Rosen*, 1993] and also contribute to polar motion variations on these timescales [*Gross et al.*, 2003]. Atmospheric surface and ocean bottom pressure fluctuations, while having only a minor influence on length-of-day variations on timescales of a few days to a few years, are the major cause of polar motion variations on these timescales [*Gross et al.*, 2003]. While processes acting between the core and mantle are thought to be the predominant source of decadal length-of-day variations [e.g., *Ponsar et al.*, 2003], decadal polar motion variations are still of unknown origin.

[3] Analyzing variation of latitude measurements taken under the auspices of the International Latitude Service (ILS) during 1900–1959, *Markowitz* [1960, 1961] deduced that at long periods the motion of the rotation pole with respect to the Earth's crust and mantle includes a periodic component superimposed on a linear drift. The periodic component, now known as the Markowitz wobble in his honor, was found to have a period of 24 years and an amplitude of 22 milliarc seconds (mas), while the linear drift was found to be 3.2 mas/year along the 60°W meridian, remarkably close to recent determinations of 3.5 mas/year along the 79°W meridian [*Gross and Vondrák*, 1999, and references therein]. The linear drift in the pole path is known to be primarily caused by glacial isostatic adjustment [e.g., *Vermeersen et al.*, 1997; *Mitrovica and Milne*, 1998], although other processes such as mantle convection [*Steinberger and O'Connell*, 1997] and secular changes in ice sheet mass accompanied by a secular change in sea

0148-0227/05/2004JB003565$09.00

level [e.g., *Trupin*, 1993; *James and Ivins*, 1997] will also contribute to the observed trend in the pole path.

[4] In recent re-reductions of the ILS and other optical astrometric measurements, which extend more than three decades past those analyzed by *Markowitz* [1960, 1961], rather than appearing as a strictly periodic phenomenon of well-defined frequency, the Markowitz wobble now appears as quasiperiodic variations in the pole path on decadal timescales having amplitudes of about 30 mas [*Gross and Vondrák*, 1999]. The cause of these decadal-scale variations in polar motion is currently unknown. The purpose of this study is to assess the degree to which redistribution of mass within the atmosphere and oceans can account for the observed decadal polar motion variations.

[5] A number of recent studies have used climate models to investigate the effects of the atmosphere and oceans on decadal polar motion variations. *Celaya et al.* [1999] used a 120-year record from the coupled atmosphere-ocean-land climate system model (CSM-1) of the National Center for Atmospheric Research (NCAR) to investigate whether or not climatic variations have enough power to excite the Markowitz wobble. They found that the atmospheric component of CSM-1 excites decadal polar motion variations that are 4 to 7 times smaller than that observed, while the variations excited by the oceanic component are about a factor of 2 smaller than that observed. Intriguingly, they also found that changes in Antarctic snowpack as modeled by the land component of CSM-1 are capable of inducing decadal polar motion variations of nearly the same amplitude as that observed. However, the period and polarization of the decadal polar motions induced by CSM-1 do not agree with those observed.

[6] *Ponte et al.* [2002] used a 240-year record from the Hadley Centre coupled climate model (HadCM2) to study oceanic excitation of decadal polar motions, finding variations having timescales of 20–30 years, similar to those observed, but having amplitudes that are about a factor of 4 smaller than those observed, and disagreeing in polarization. They also found oceanic excitation of decadal length-of-day variations to have amplitudes less than 0.1 milliseconds (ms).

[7] *de Viron et al.* [2004] used a 130-year record from a general circulation model of the atmosphere from the Hadley Centre that was forced by sea surface temperature and global ice conditions to study atmospheric excitation of decadal length-of-day and polar motion variations. For the length of day, they found significant coherence with the observed variations in the 9–12 year and 13–23 year period bands, but amplitudes that are 4 to 5 times smaller than those observed. For polar motion, they found only a very small effect of the atmosphere on variations that have periods greater than 10 years.

[8] Climate models such as those used by *Celaya et al.* [1999] and *Ponte et al.* [2002] capture contemporary climatic conditions and hence can be used to study contemporary climatic variability in the atmosphere-ocean system and to predict the effects of such variability on the Earth's rotation. However, unlike weather prediction models, climate models do not represent the state of the atmosphere and oceans at any given epoch, and hence can be used to study climatic variability in the atmosphere-ocean system in a statistical sense only. Data assimilating weather prediction models, such as the operational model of the National Centers for Environmental Prediction (NCEP) or the NCEP/NCAR reanalysis model, do represent the state of the atmosphere at specific epochs and hence can be used to study atmospheric excitation of Earth orientation variations during a specific time interval. When the products of such atmospheric models are used to force ocean models, oceanic excitation during the same time interval can also be studied. *Brzezinski et al.* [2002, 2005] have used this approach to study atmospheric and oceanic excitation of polar motion on interannual to decadal timescales during 1950–1999 using atmospheric results from the NCEP/NCAR reanalysis system and oceanic results from the Simple Ocean Data Assimilation (SODA) system of *Carton et al.* [2000], finding that atmospheric and oceanic excitation cannot explain the observed long-period polar motion excitation variations.

[9] Here, atmospheric and oceanic excitation of decadal-scale Earth orientation variations during 1949–2002 is studied using an atmospheric angular momentum series computed from the NCEP/NCAR reanalysis system and an oceanic angular momentum series computed from a near-global ocean model forced by surface fluxes from the NCEP/NCAR reanalysis system. While the emphasis of this study is on atmospheric and oceanic excitation of the Markowitz wobble during 1949–2002, the contribution of atmospheric and oceanic processes to exciting decadal length-of-day variations during this time period will also be investigated.

2. Earth Orientation Variations

[10] The rotation of the solid Earth changes in response to both the action of torques acting on the solid Earth and to changes in the mass distribution of the solid Earth. Observed changes in the Earth's rotation can be studied using the principle of conservation of angular momentum, which in a rotating, body-fixed terrestrial reference frame is given by:

$$\frac{\partial \mathbf{L}}{\partial t} + \boldsymbol{\omega} \times \mathbf{L} = \boldsymbol{\tau} \tag{1}$$

where $\boldsymbol{\omega}$ is the Earth's rotation vector, $\mathbf{L}$ is its angular momentum vector, and $\boldsymbol{\tau}$ are the torques acting on the Earth. In general, the angular momentum vector $\mathbf{L}(t)$ can be written as the sum of a term $\mathbf{h}(t)$ due to motion relative to the rotating reference frame and of a term that includes changes in the inertia tensor $\mathsf{I}(t)$ of the body caused by changes in the distribution of mass:

$$\mathbf{L} = \mathsf{I} \cdot \boldsymbol{\omega} + \mathbf{h} \tag{2}$$

[11] The Earth's rotation deviates only slightly from a state of uniform rotation, the deviation being a few parts in 10^8 in speed, corresponding to changes of a few milliseconds in the length of the day, and about a part in 10^6 in the orientation of the rotation axis relative to the crust of the Earth, corresponding to a variation of several hundred milliarc seconds in polar motion. Such small deviations in rotation can be studied by linearizing equations (1) and (2). Let the Earth initially be uniformly rotating at the rate Ω

about its figure axis and orient the rotating, body-fixed terrestrial reference frame so that its z axis is aligned with the figure axis. Under a small perturbation to this initial state, the relative angular momentum $\mathbf{h}$ will be perturbed to $\mathbf{h} + \Delta\mathbf{h}$, the inertia tensor $\mathbf{I}$ will be perturbed to $\mathbf{I} + \Delta\mathbf{I}$, and the angular velocity vector $\boldsymbol{\omega}$ will be perturbed to $\boldsymbol{\omega} + \Delta\boldsymbol{\omega}$, where

$$\boldsymbol{\omega} + \Delta\boldsymbol{\omega} = \Omega \left[m_x(t), m_y(t), 1 + m_z(t)\right]^{\mathrm{T}} \tag{3}$$

where the initial rate of rotation Ω is taken to be the mean angular velocity of the Earth (7.292115×10^{-5} rad/s) and the Ωm_i are the elements of the perturbation $\Delta\boldsymbol{\omega}$ to the rotation vector. Keeping terms to first order in perturbed quantities, and considering excitation mechanisms such as atmospheric surface and oceanic bottom pressure variations that load the solid Earth at its surface causing it to deform, the axial and equatorial components of equation (1) can be written in the absence of external torques as [e.g., *Munk and MacDonald*, 1960; *Wahr*, 1982; *Barnes et al.*, 1983; *Eubanks*, 1993; *Dickman*, 2003]

$$\Delta\Lambda(t) = \frac{\Lambda_o}{C_m\Omega}\left[\Delta h_z(t) + 0.756\Omega\Delta I_{zz}(t)\right] \tag{4}$$

$$\mathbf{m}(t) + \frac{i}{\sigma_o}\frac{d\mathbf{m}(t)}{dt} = \boldsymbol{\chi}(t) - \frac{i}{\Omega}\frac{d\boldsymbol{\chi}(t)}{dt} \tag{5}$$

where the change $\Delta\Lambda(t)$ in the length of the day is related to $m_z(t)$ by $\Delta\Lambda(t)/\Lambda_o = -m_z(t)$, Λ_o is the nominal length of day of 86,400 s, C_m is the polar moment of inertia of the Earth's crust and mantle (7.1242×10^{37} kg m^2), the factor of 0.756 accounts for the yielding of the crust and mantle due to the imposed surface loads, $\mathbf{m}(t) \equiv m_x(t) + i\, m_y(t)$, where $m_x(t)$ and $m_y(t)$ are the direction cosines of the Earth's rotation axis relative to the axes of the rotating, body-fixed reference frame (see equation (3)), and $\sigma_o \equiv 2\pi/T_o(1 + i/2Q_o)$ is the complex-valued frequency of the Chandler wobble that has a period of T_o and a resonance quality factor of Q_o. In the absence of external torques, the $\boldsymbol{\chi}(t)$ in equation (5), known as the polar motion excitation functions, are functions of changes in relative angular momentum and of changes in the Earth's inertia tensor [*Wahr*, 1982]:

$$\boldsymbol{\chi}(t) = \frac{1.61}{\Omega\,(C - A)}\left[\Delta\mathbf{h}(t) + \frac{\Omega\,\mathbf{c}(t)}{1.44}\right] \tag{6}$$

where $\Delta\mathbf{h}(t) \equiv \Delta h_x(t) + i\,\Delta h_y(t)$ with $\Delta h_x(t)$ and $\Delta h_y(t)$ being the x and y components, respectively, of the perturbation to the relative angular momentum, $\mathbf{c}(t) \equiv \Delta I_{xz}(t) + i\,\Delta I_{yz}(t)$ with $\Delta I_{xz}(t)$ and $\Delta I_{yz}(t)$ being the perturbation to the two indicated elements of the Earth's inertia tensor, C and A are the greatest and least, respectively, principal moments of inertia of the Earth with $C-A$ being 2.61×10^{35} kg m^2, the factor of 1.44 accounts for the yielding of the solid Earth due to the imposed surface loads, and the factor of 1.61 includes the effect of core decoupling.

[12] Equations (5) and (6) relate changes in equatorial angular momentum to changes in the location of the Earth's rotation pole. However, observations of the Earth's rotation, as reported by Earth rotation services, do not give the location of the Earth's rotation pole but rather give the location of the celestial intermediate pole within the rotating, body-fixed terrestrial reference frame [*Brzezinski*, 1992; *Gross*, 1992]. Writing equation (5) in terms of the reported polar motion parameters yields:

$$\mathbf{p}(t) + \frac{i}{\sigma_o}\frac{d\mathbf{p}(t)}{dt} = \boldsymbol{\chi}(t) \tag{7}$$

where $\mathbf{p}(t) \equiv p_x(t) - i\,p_y(t)$ with $p_x(t)$ and $p_y(t)$ being the x and y components, respectively, of the reported location of the celestial intermediate pole within the terrestrial reference frame with, by convention, $p_y(t)$ being positive toward 90°W longitude. Note that at frequencies much less than Ω, the right-hand side of equation (5) becomes the same as that of equation (7), so the motion of the celestial intermediate pole is the same as that of the rotation pole at low frequencies.

[13] Assuming a time dependence of $e^{i\omega t}$, equation (7) can be written in the frequency domain as:

$$\mathbf{P}(\omega) = \frac{\sigma_o}{\sigma_o - \omega}\boldsymbol{\chi}(\omega) \tag{8}$$

At frequencies much less than the Chandler frequency, such that $\omega \ll \mathrm{Re}(\sigma_o)$, equation (8) reduces to $\mathbf{P}(\omega) = \boldsymbol{\chi}(\omega)$, showing that the low-frequency motion of the celestial intermediate pole $\mathbf{P}(\omega)$ is the same as the low-frequency motion of the excitation pole $\boldsymbol{\chi}(\omega)$. By similar reasoning applied to equation (5), the low-frequency motion of the rotation pole $\mathbf{M}(\omega)$ can also be shown to be the same as that of the excitation pole. Thus, at sufficiently low frequencies, the celestial intermediate pole, the rotation pole, and the excitation pole all have the same motion.

[14] In this study, equations (4) and (7) will be used to compare observed decadal length-of-day and polar motion excitation variations, respectively, with modeled variations computed using the products of atmospheric and oceanic general circulation models. Observed polar motion excitation functions will be computed from polar motion observations $\mathbf{p}(t)$ using equation (7). Modeled length-of-day and polar motion excitation variations will be computed from modeled changes in the angular momentum of atmospheric winds and surface pressure and oceanic currents and bottom pressure. The relative importance of these processes to exciting decadal Earth orientation variations will then be assessed by comparing the modeled with the observed variations in both the time and frequency domains.

3. Data Sets

3.1. Observed Earth Orientation Variations

[15] The observed polar motion excitation and length-of-day (LOD) series used in this study are those derived from an extended version of the COMB2002 Earth orientation series [*Gross*, 2003]. COMB2002 is a combination of Earth orientation measurements taken by the techniques of optical astrometry, lunar and satellite laser ranging, very long baseline interferometry, and the global positioning system. Besides estimating Universal Time (UT1) and polar motion,

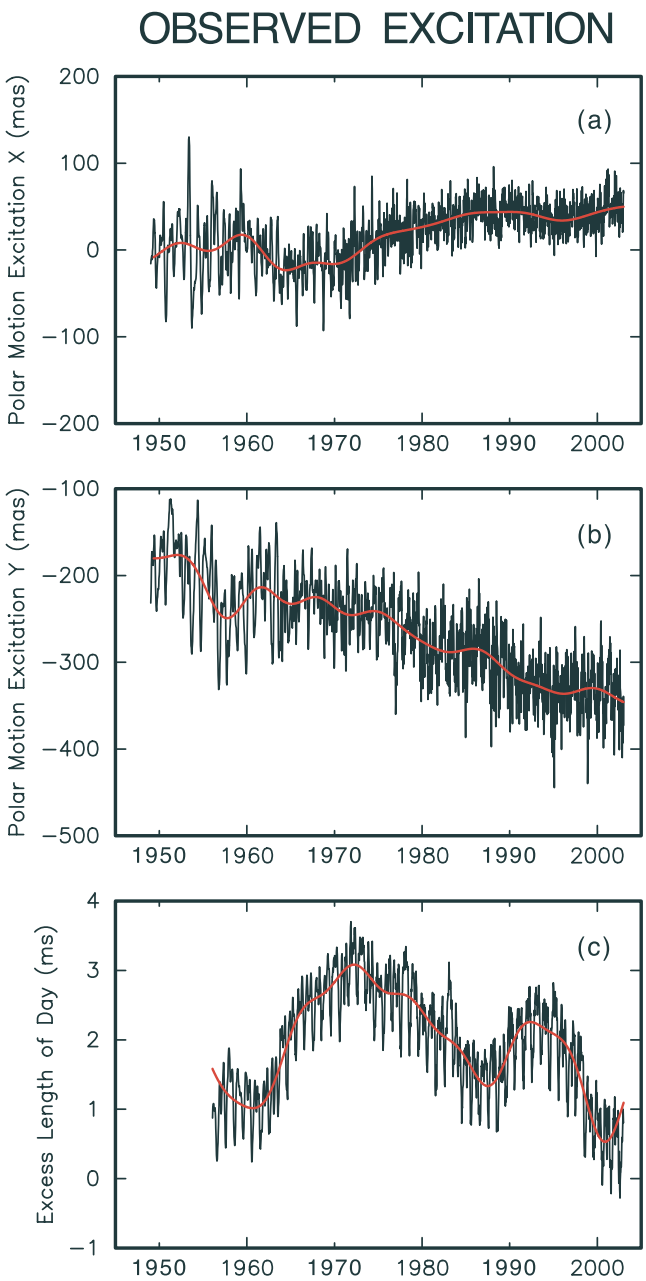

Figure 1. Extended COMB2002 series of observed (a, b) polar motion excitation and (c) length-of-day variations from which tidal effects have been removed (black). The decadal-scale variations in these series, obtained by applying to them a low-pass filter with a cutoff period of 6 years, are shown in red. The mean and trend have not been removed from the displayed series.

the Kalman filter used to combine the measurements also self-consistently estimates their time rates of change [*Gross et al.*, 1998] and hence the length-of-day and polar motion excitation functions. The COMB2002 length-of-day and polar motion excitation series span 20 January 1962 to 11 January 2003 at daily intervals.

[16] In order to match the time span of the atmospheric and oceanic angular momentum series, which begin in 1948 and 1949, respectively (see below), the COMB2002 length-of-day and polar motion excitation series were extended back to 1948 using the Hipparcos optical astrometric Earth orientation series [*Vondrák et al.*, 1998]. The final Hipparcos star catalog was used by *Vondrák et al.* [1998] to re-reduce all available optical astrometric measurements of star positions taken since 1900 using modern standards and data reduction methods. The resulting Hipparcos Earth orientation series consists of polar motion values spanning 1900–1991 at 5-day intervals, with UT1 values being given since the introduction of atomic clocks in 1956.

[17] Prior to using the Hipparcos Earth orientation series to extend COMB2002 back to 1948, corrections to its bias, rate, annual component, and stated uncertainties were applied in order to make it consistent with COMB2002. These corrections to the Hipparcos series were determined by procedures similar to those used to correct the Bureau International de l'Heure (BIH) optical astrometric series used in COMB2002 [*Gross*, 2003]. After adjustment, the independent portion of the Hipparcos optical astrometric series was combined with COMB2002 to obtain the extended COMB2002 Earth orientation series whose polar motion excitation values span 1 January 1948 to 11 January 2003 at daily intervals, with the length-of-day values being given since 19 January 1956.

[18] Tidal effects have been removed from the extended COMB2002 length-of-day values using the model of *Yoder et al.* [1981] for the long-period solid Earth tides and the model of *Kantha et al.* [1998] for the long-period ocean tides; the empirical model of *Gross et al.* [1997] was used to remove the effect of the termensual (9.12- and 9.13-day), fortnightly (13.63- and 13.66-day), and monthly (27.55-day) ocean tides from the extended COMB2002 polar motion excitation values. In order to match the temporal resolution of the oceanic angular momentum series (see below), 10-day averages of the daily extended COMB2002 polar motion excitation and LOD series were formed by summing 11 consecutive values using weights of 1/20, 1/10, . . ., 1/10, 1/20. The resulting observed 10-day-averaged nontidal polar motion excitation and length-of-day series are shown as the black curves in Figure 1 with the red curves showing the decadal variations that were obtained by applying to the series a low-pass filter having a cutoff period of 6 years.

3.2. Atmospheric Angular Momentum

[19] The atmospheric angular momentum (AAM) series used in this study is that derived from the NCEP/NCAR reanalysis project [*Kalnay et al.*, 1996] and was obtained from the International Earth Rotation and Reference Systems Service (IERS) Special Bureau for the Atmosphere (SBA [*Salstein et al.*, 1993]). Both the angular momentum due to winds, computed by integrating the horizontal winds from the surface to the top of the model at 10 hPa [*Salstein and Rosen*, 1997], and the angular momentum due to surface pressure variations, computed by assuming that the oceans respond as an inverted barometer to the imposed surface pressure variations, were used here. The NCEP/NCAR reanalysis AAM series available from the IERS SBA spans 1 January 1948 to the present at 6-hour intervals. Daily averages of the 6-hour values were first formed by summing 5 consecutive values using weights of 1/8, 1/4, 1/4, 1/4, 1/8. In order to match the temporal resolution of the oceanic

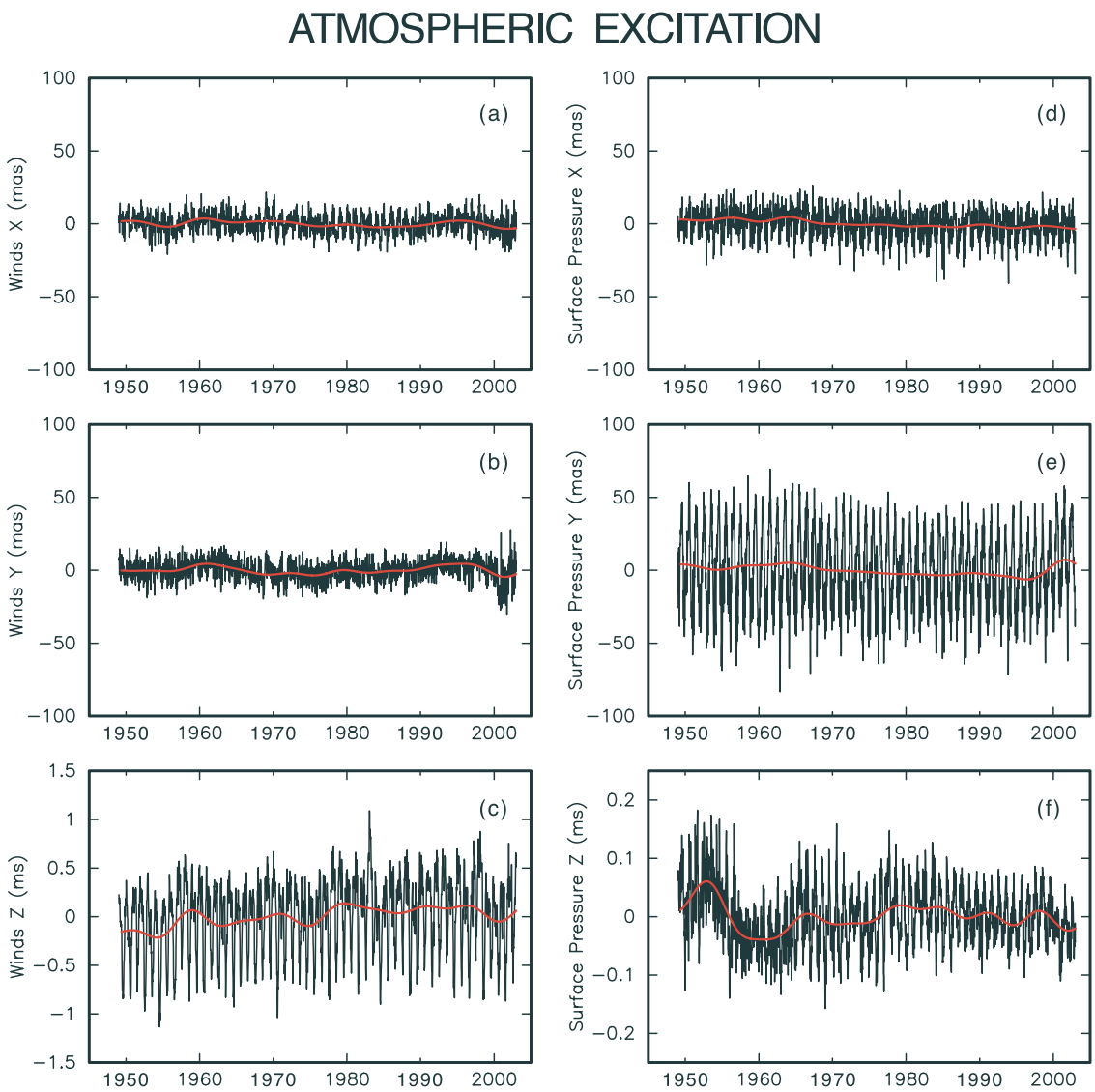

Figure 2. Modeled (a, b, d, e) polar motion excitation and (c, f) length-of-day variations caused by changes in atmospheric winds (Figures 2a, 2b, and 2c) and surface pressure (Figures 2d, 2e, and 2f) during 1949–2002 from the NCEP/NCAR reanalysis project (black). Decadal-scale variations in these series, obtained by applying to them a low-pass filter with a cutoff period of 6 years, are shown in red. The excitation associated with atmospheric surface pressure variations has been computed by assuming that the oceans respond as an inverted barometer to the imposed surface pressure variations. The mean, but not the trend, has been removed from the displayed series. Note the different scales of Figures 2c and 2f.

angular momentum series (see below), 10-day averages of the daily AAM series were then formed by summing 11 consecutive values using weights of 1/20, 1/10, …, 1/10, 1/20. The resulting 10-day-averaged AAM series, which have been converted to equivalent length-of-day and polar motion excitation functions, are shown as the black curves in Figure 2 with the red curves showing the decadal variations that were obtained by applying to the series a low-pass filter having a cutoff period of 6 years.

3.3. Oceanic Angular Momentum

[20] The oceanic angular momentum (OAM) series used in this study has been computed here from the results of a simulation of the general circulation of the oceans done at JPL as part of their participation in the Estimating the Circulation and Climate of the Ocean (ECCO) consortium [*Stammer et al.*, 2002]. The ocean model used in this simulation is based on the MIT ocean general circulation model (MITgcm) [*Marshall et al.*, 1997a, 1997b] and has realistic boundaries and bottom topography, 46 vertical levels ranging in thickness from 10 m at the surface to 400 m at depth using height as the vertical coordinate, and spans the globe between 78°S to 80°N latitude with a latitudinal grid spacing ranging from 1/3° at the equator to 1° at high latitudes and a longitudinal grid spacing of 1°. The simulation is initialized with mean January temperature and salinity distributions from the World Ocean Database 1998 (WOD98) [*Conkright et al.*, 1999] and is spun-up

from rest for 20 years using repeated 1949 surface fluxes from the NCEP/NCAR reanalysis project (twice daily wind stress and daily surface heat flux and evaporation-precipitation fields). The model is subsequently forced with 1949–2002 surface fluxes from the NCEP/NCAR reanalysis project. In addition to NCEP/NCAR surface fluxes, time-mean river runoff is prescribed as by *Stammer et al.* [2004], model surface temperature is relaxed to daily sea surface temperature from the NCEP/NCAR reanalysis with a relaxation period of 30 days, and model surface salinity is relaxed to monthly WOD98 sea surface salinity with a relaxation period of 45 days.

[21] The simulation employs the K-Profile Parameterization (KPP) vertical mixing scheme of *Large et al.* [1994] and the isopycnal mixing schemes of *Redi* [1982] and of *Gent and McWilliams* [1990] with surface tapering as per *Large et al.* [1997]. Laplacian diffusion and friction are used except for horizontal friction, which is biharmonic. Lateral boundary conditions are closed. No-slip bottom, free-slip lateral, and implicit free surface boundary conditions are employed. Surface freshwater fluxes, including the evaporation-precipitation fields and time-mean river runoff, are applied as virtual salt fluxes in which the model's surface salinity is modified in accordance to the freshwater forcing as opposed to changing the model's freshwater volume. Because the ocean model is integrated in a volume-preserving configuration (Boussinesq approximation), virtual salt fluxes cause artificial mass variations that are subsequently removed (see below) using the method of *Greatbatch* [1994]. Empirical mixing coefficients follow those of *Menemenlis et al.* [2005]: isopycnal diffusivity and isopycnal thickness diffusivity is 750 m^2/s, horizontal viscosity is 10^{12} m^4/s, background vertical diffusivity and viscosity are 1.5×10^{-5} m^2/s and 1.8×10^{-5} m^2/s, respectively, the critical bulk Richardson number, which sets boundary layer depth, is $Ri_c = 0.354$, and the threshold gradient Richardson number, which controls shear instability vertical mixing, is $Ri_0 = 0.699$.

[22] A novel aspect of the ocean model as configured for this simulation is that the bottom cells have been lopped [*Adcroft et al.*, 1997]. With lopped cells, instead of restricting steps in bottom topography to be one of the 46 vertical steps, partial steps are allowed. In this simulation, cells are lopped by up to 70% provided the residual thickness is greater than 50 m. Partial steps represent the bottom topography better and hence improves the accuracy of the modeled ocean bottom pressure variations and thus the accuracy of the angular momentum due to bottom pressure variations.

[23] Atmospheric surface pressure was not used to force the ocean model. At periods greater than a few days, and certainly on the decadal timescales of interest in this study, the predominant response of the oceans to surface pressure forcing is a simple static response like that of an inverted barometer [*Wunsch and Stammer*, 1997]. The static response of the oceans to changes in atmospheric surface pressure has been taken into account here during the computation of the atmospheric angular momentum (see section 3.2).

[24] Since the configuration of the MITgcm used in this study uses the Boussinesq approximation [*Marshall et al.*, 1997a, 1997b], it conserves volume rather than mass. Artificial mass variations can be introduced into Boussinesq models because of the applied surface heat and salt fluxes. For example, the changing applied heat flux will change the density, which, since volume is conserved, will artificially change the mass of the modeled oceans. If left uncorrected, this artificial mass change will cause artificial changes to the ocean bottom pressure and hence to the angular momentum associated with ocean bottom pressure variations. Following the suggestion of *Greatbatch* [1994], mass conservation has been enforced here by adding to the sea surface a spatially uniform layer of just the right fluctuating thickness. The angular momentum associated with ocean bottom pressure variations has been corrected for the effects of artificial mass variations in the MITgcm by computing the effect on the angular momentum of this spatially uniform mass-conserving layer.

[25] The angular momentum carried by oceanic currents was computed here by integrating the zonal $u(\mathbf{r}, t)$ and meridional $v(\mathbf{r}, t)$ currents throughout the volume V_o of the modeled oceans:

$$\mathbf{L_c}(t) = -\int_{V_o} \rho(\mathbf{r},t) r [\sin\phi u(\mathbf{r},t) + iv(\mathbf{r},t)] e^{i\lambda} dV \tag{9}$$

$$L_{c,z}(t) = \int_{V_o} \rho(\mathbf{r},t)\, r\, \cos\,\phi u(\mathbf{r},t) dV \tag{10}$$

where $\mathbf{L_c}(t) \equiv L_{c,x}(t) + i\, L_{c,y}(t)$ with $L_{c,x}(t)$, $L_{c,y}(t)$, and $L_{c,z}(t)$ being the x, y, and z components, respectively, of the angular momentum due to currents, ϕ is north latitude, λ is east longitude, and $\rho(\mathbf{r}, t)$ is the density of some mass element located at position $\mathbf{r}$. The angular momentum due to changes in the mass distribution of the oceans, or, equivalently, due to changes in ocean bottom pressure, was computed here by integrating the time-dependent density field throughout the volume of the modeled oceans:

$$\mathbf{L_p}(t) = -\Omega \int_{V_o} \rho(\mathbf{r},t) r^2\, \sin\phi\, \cos\phi e^{i\lambda} dV \tag{11}$$

$$L_{p,z}(t) = \Omega \int_{V_o} \rho(\mathbf{r},t) r^2 \cos^2\phi dV \tag{12}$$

where $\mathbf{L_p}(t) \equiv L_{p,x}(t) + i\, L_{p,y}(t)$ with $L_{p,x}(t)$, $L_{p,y}(t)$, and $L_{p,z}(t)$ being the x, y, and z components, respectively, of the angular momentum due to mass redistribution. When using equations (9)–(12) to calculate the OAM, the effects of enforcing mass conservation and of changes in sea surface height were both included.

[26] The axial components of the modeled oceanic angular momentum values were converted to equivalent length-of-day variations using equation (4) with $\Delta h_z(t) \equiv L_{c,z}(t)$ and with $\Omega \Delta I_{zz}(t) \equiv L_{p,z}(t)$; the equatorial components were converted to equivalent polar motion excitation functions using equation (6) with $\Delta\mathbf{h}(t) \equiv \mathbf{L_c}(t)$ and $\Omega\mathbf{c}(t) \equiv \mathbf{L_p}(t)$. The resulting modeled oceanic excitation functions, which span 1949–2002 at 10-day intervals, are shown as the black curves in Figure 3 with the red curves showing the decadal variations that were obtained by

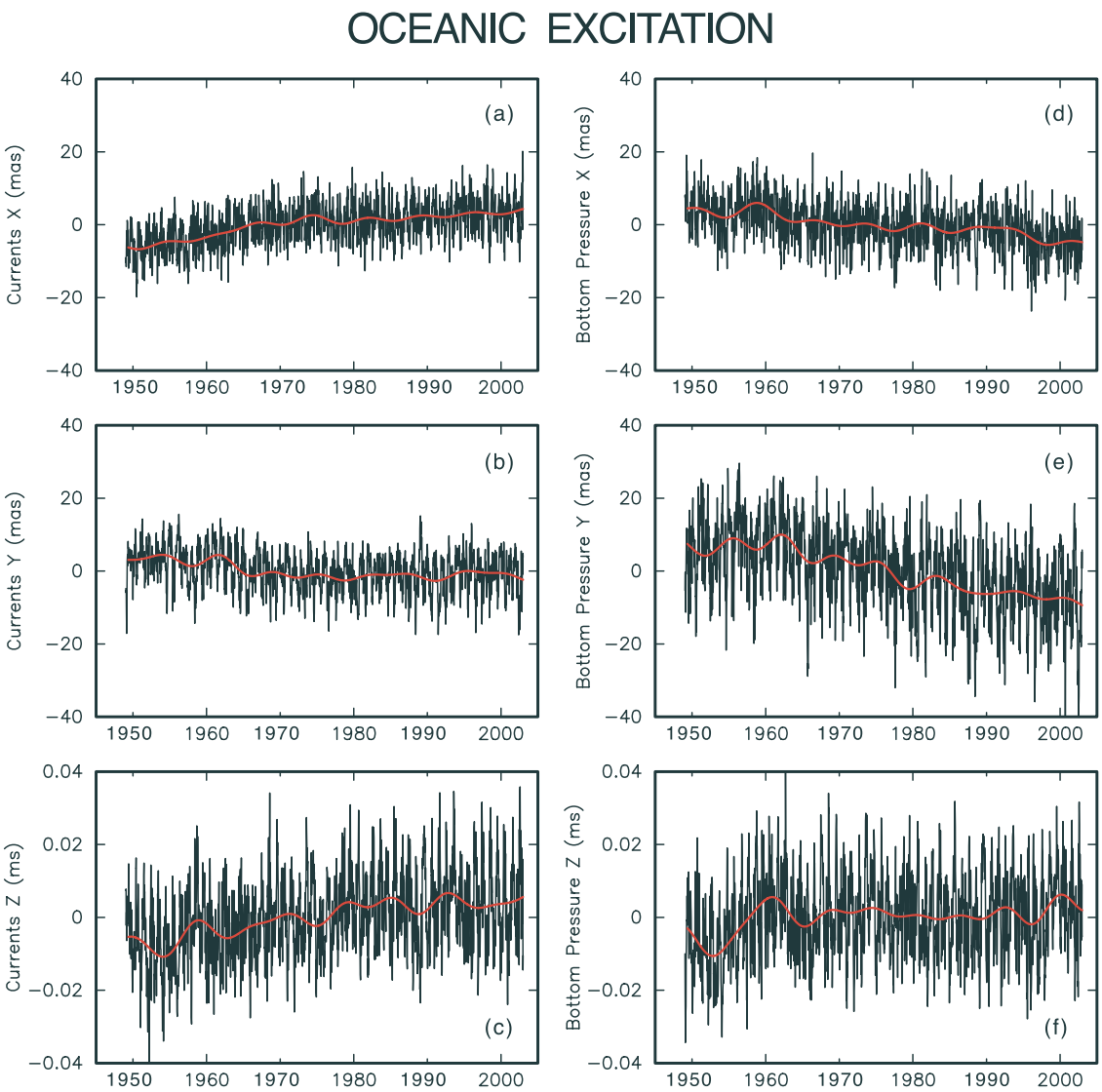

Figure 3. Modeled (a, b, d, e) polar motion excitation and (c, f) length-of-day variations caused by changes in oceanic currents (Figures 3a, 3b, and 3c) and bottom pressure (Figures 3d, 3e, and 3f) during 1949–2002 (black). Decadal-scale variations in these series, obtained by applying to them a low-pass filter with a cutoff period of 6 years, are shown in red. The mean, but not the trend, has been removed from the displayed series.

applying to the series a low-pass filter having a cutoff period of 6 years.

4. Decadal Variations

[27] Figure 4 compares the observed decadal-scale variations in polar motion excitation and length of day (black curves) with those caused by the sum of atmospheric winds and surface pressure (red curves) as well as with those caused by the sum of atmospheric winds and surface pressure and oceanic currents and bottom pressure (blue curves). In order to focus on the decadal variations, and since the trend in the pole path is known to be largely caused by glacial isostatic adjustment, a mean and trend have been removed from all the series displayed in Figure 4. As expected, because of the dominance of processes acting between the core and mantle in causing decadal length-of-day variations, the variations caused by the atmosphere and oceans is much smaller than those observed (Figure 4c). While the observed peak-to-peak variations in the length of day on decadal timescales during 1956–2002 are about 2.2 ms, the peak-to-peak variations caused by the sum of all the modeled atmospheric and oceanic processes are only about 0.3 ms, or about 14% of the observed variations, with atmospheric winds (not shown) being the major contributor.

[28] Figures 4a and 4b show that atmospheric and oceanic excitation of polar motion on decadal timescales during 1949–2002 is also much smaller than that observed. While the observed peak-to-peak variations in the x and y components of polar motion excitation on decadal timescales during 1949–2002 are about 45 mas and 60 mas, respectively, the peak-to-peak variations caused by the sum of all the modeled atmospheric and oceanic processes are only

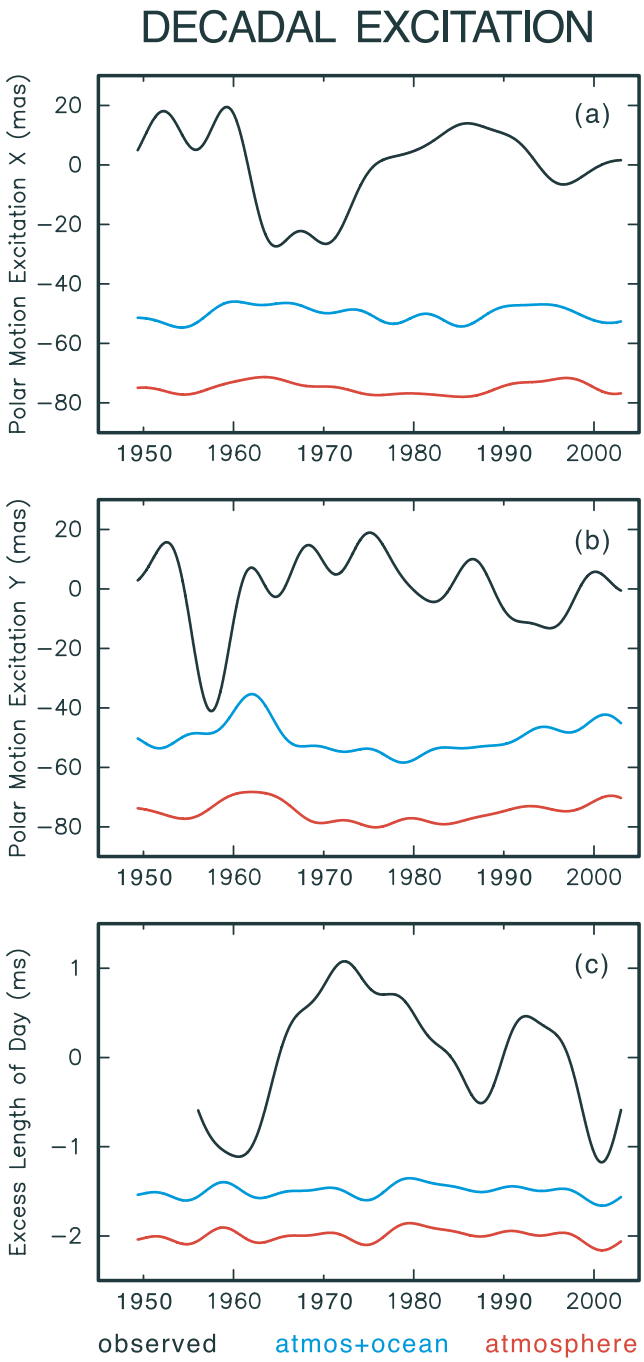

Figure 4. Observed (a, b) polar motion excitation and (c) length-of-day variations (black curves), variations caused by the modeled atmospheric winds and surface pressure (red curves), and variations caused by the sum of the modeled atmospheric winds, surface pressure, oceanic currents, and bottom pressure (blue curves) on decadal timescales. The atmospheric surface pressure term is that computed assuming the oceans respond as an inverted barometer to the imposed surface pressure variations. The trend has been removed from all series. For clarity of display, the curves have been shifted vertically so that they do not overlap with each other.

about 9 mas and 23 mas, or about 20% and 38% of the observed variations, respectively.

[29] Power spectra and coherence magnitude and phase of the observed, atmospheric, and sum of atmospheric and oceanic polar motion excitation functions are shown in Figure 5. The atmospheric excitation function includes the contributions of both wind and surface pressure variations where the response of the oceans to the surface pressure changes is assumed to be that of an inverted barometer. The oceanic excitation function includes the contributions of both currents and ocean bottom pressure variations. The spectra have been computed by the multitaper method [*Percival and Walden*, 1993] using a resolution bandwidth of $2f_R$, where $f_R \equiv 1/N\Delta t$ is the fundamental, or Rayleigh, frequency with N being the number of samples in the time series (1960), Δt being the sampling interval (10 days), and hence $N\Delta t$ being the length of the time series (54 years). A simple unweighted average of the resulting first 3 eigenspectra was then formed to obtain the spectra shown in Figure 5a. The coherence and phase estimates shown in Figures 5b and 5c, respectively, were obtained by averaging over 11 frequency intervals and the 95% and 99% confidence limits of the squared magnitude of the coherence are indicated by the horizontal dashed lines in Figure 5b. Only the low-frequency portion of the spectra and coherence magnitude and phase are shown in Figure 5.

[30] As shown in Figure 5a, better agreement with the observed power at frequencies less than 3 cpy is obtained when the effects of oceanic current and bottom pressure variations is added to that of atmospheric wind and surface pressure changes, although discrepancies still remain, particularly at retrograde frequencies. Large discrepancies in power also exist at frequencies near 0 cpy, indicating that atmospheric and oceanic processes do not have enough power to excite decadal-scale polar motion variations to their observed level. At the very lowest frequencies, Figure 5b shows that the modeled atmospheric and oceanic excitation functions are just barely significantly coherent with the observed excitation, but Figure 5c shows that at these lowest frequencies the modeled and observed excitation functions are nearly 180° out of phase.

5. Evaluation of Observed and Modeled Series

5.1. Optical Astrometric Measurements

[31] The polar motion excitation observations used in this study are from an extended version of the COMB2002 combined Earth orientation series. Polar motion measurements from the accurate space-geodetic techniques do not regularly contribute to this series until the start of the LAGEOS satellite laser ranging data set in 1976 (although lunar laser ranging measurements from the McDonald station start earlier than this, they are not of UT1 and polar motion, but are rather of UT0 and variation of latitude). Prior to 1976, the extended COMB2002 polar motion excitation series is based upon less accurate optical astrometric measurements, with the Hipparcos series of *Vondrák et al.* [1998] being used from 1948 to 1961 and the BIH series of *Li and Feissel* [1986] being used from 1962 to 1981 [*Gross*, 2003].

[32] While the accurate space-geodetic polar motion measurements are free of systematic error, the less accurate

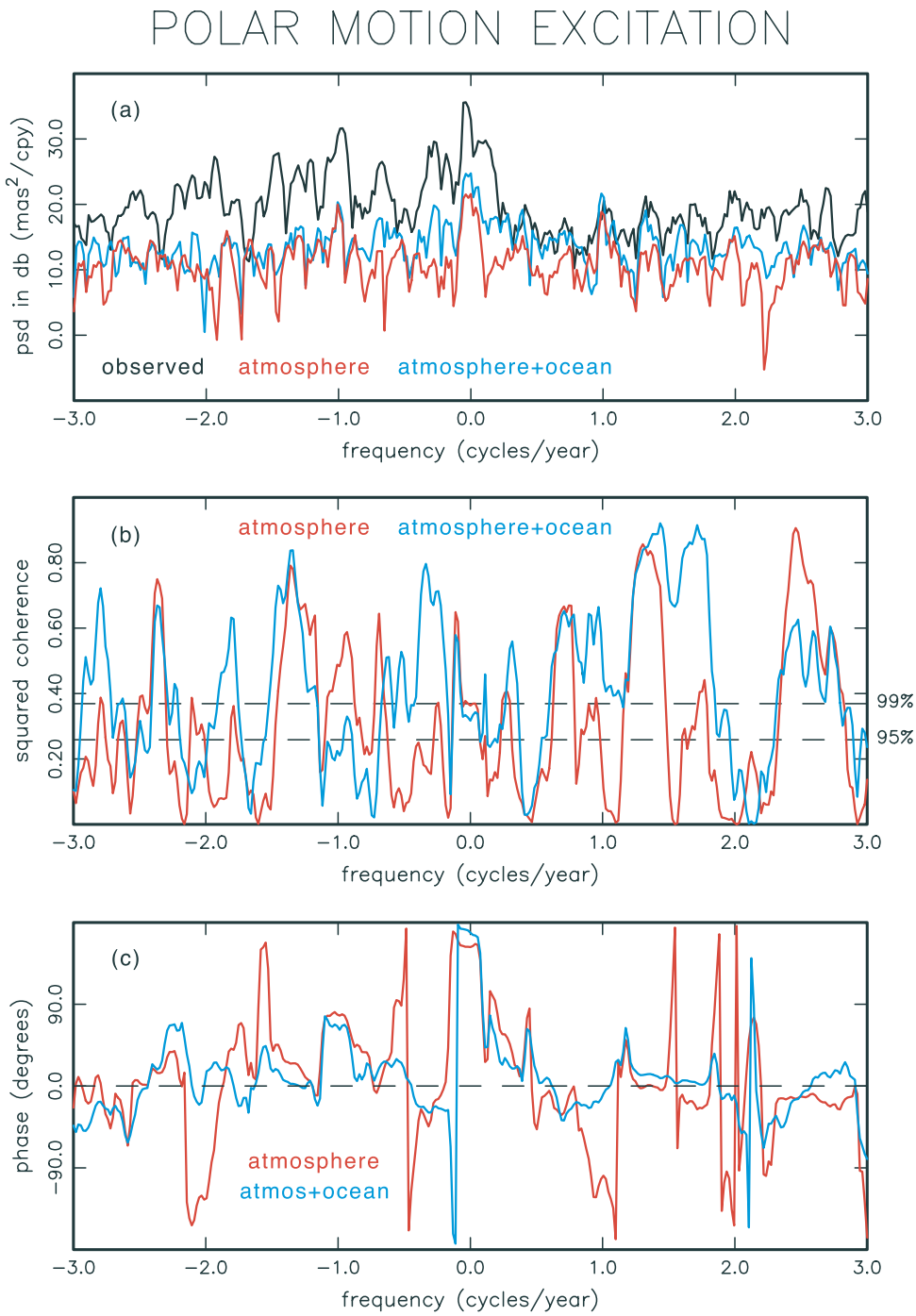

Figure 5. (a) Power spectral density (psd) estimates in decibels (dB) of the observed polar motion excitation variations during 1949–2002 (black curve), of the variations due to atmospheric wind and surface pressure changes (red curve), and of the variations due to the sum of wind, surface pressure, oceanic currents, and ocean bottom pressure changes (blue curve). (b) Squared magnitude of the coherence and (c) the phase, respectively, between the observed variations and either the variations due to atmospheric wind and surface pressure changes (red curves) or the variations due to the sum of wind, surface pressure, oceanic currents, and ocean bottom pressure changes (blue curves). The retrograde component of polar motion excitation is represented by negative frequencies, the prograde component by positive frequencies. The horizontal dashed lines in Figure 5b indicate the 95% and 99% confidence levels of the magnitude of the squared coherence. A mean, a trend, and variations at the annual (1 cpy), semiannual (2 cpy), and terannual (3 cpy) frequencies have been removed from the data sets prior to spectral and coherence estimation.

optical astrometric measurements are not. In fact, prior to being assimilated into COMB2002 and its extension, the annual terms of the BIH and Hipparcos optical astrometric series were adjusted to agree in amplitude and phase with that of the space-geodetic series used in COMB2002 [*Gross*, 2003] in order to correct for systematic, seasonally varying effects that are known to be present in optical astrometric measurements.

[33] Such systematic errors may corrupt more than just the seasonal signals. *Gross and Vondrák* [1999, Figure 1] compared the decadal variations evident in the International Latitude Service (ILS), Hipparcos, and SPACE96 polar motion series. Since the ILS optical astrometric measurements were used in generating the Hipparcos series, the decadal variations evident in these two series were found by them to be in reasonably good agreement with each other. However, they found little agreement between the decadal polar motion variations evident in the SPACE96 combined space-geodetic series with those evident in either the ILS or Hipparcos optical astrometric series. The decadal polar motion variations of the SPACE96 series were of smaller amplitude and had a different phase than did those of either the ILS or Hipparcos series. This discrepancy between the decadal polar motion variations evident in the less accurate ILS and Hipparcos series with those evident in the highly accurate SPACE96 series raises serious concerns about the reality of the decadal variations exhibited by the ILS and Hipparcos optical astrometric series, and hence about the reality of the decadal variations exhibited prior to 1976 in the extended COMB2002 polar motion excitation series.

[34] In view of this concern about the accuracy of the decadal polar motion variations evident in optical astrometric measurements, comparisons of modeled and observed variations should be restricted to just the time period spanned by the space-geodetic measurements, that is, after about 1976. Figures 4a and 4b show that the modeled polar motion excitation variations have a much smaller amplitude than do the observed variations during 1976–2002, just like they do during 1949–2002. While the observed (black curves) peak-to-peak variations about the best fitting trend in the x and y components of polar motion excitation on decadal timescales during 1976–2002 are about 25 mas and 30 mas, respectively, the peak-to-peak variations about the trend caused by the sum of all the modeled atmospheric and oceanic processes (blue curves) are only about 7 mas and 4 mas, or about 28% and 13% of the observed variations, respectively. So, even though the observed polar motion excitation functions become more accurate after 1976, there is still very little agreement on decadal timescales with the modeled variations. This lack of agreement between the modeled and observed polar motion excitation series on decadal timescales during 1976–2002 is consistent with the results of *Gross et al.* [2003], who found little agreement during 1980–2000 between the observed decadal polar motion excitation variations and those modeled by atmospheric and oceanic processes, with the power of the modeled variations being much less than the power of the observed variations.

5.2. Ocean Models

[35] The oceanic angular momentum series used in this study is from a near-global ocean model forced by NCEP/NCAR surface fluxes during 1949–2002. As mentioned earlier, a novel aspect of the configuration of this ocean model is the use of lopped cells, which are meant to improve the representation of the bottom topography and hence the accuracy of the modeled ocean bottom pressure fields and thus the accuracy of the angular momentum due to changes in ocean bottom pressure. In order to evaluate the impact of lopped cells on the accuracy of the modeled oceanic angular momentum, this and two other OAM series are compared in Figure 6 to observed polar motion excitation functions from which atmospheric effects have been removed using the NCEP/NCAR reanalysis AAM series. The two other OAM series used in this comparison are another simulation series similar to the 50-year series used here but which is from a model that did not use lopped cells, and a data assimilative series that is from a model that also did not use lopped cells. The other simulation series, whose series designator is c20010701 but which is denoted as the 20-year series in Figure 6 and which is the same series as that studied by *Gross et al.* [2003], is from an ocean model that has the same spatial resolution and forcing as the 50-year series studied here, but that does not use lopped cells and that extends only from 74°S to 74°N latitude. The data assimilative series, whose series designator is kf049f and which is denoted as the assimilative series in Figure 6, is from an ocean model that has the same model configuration and forcing as the 20-year series but that is also constrained by altimetric measurements of sea surface height and by expendable bathythermograph (XBT) data. Since the data assimilative series begins in 1993 with the start of the TOPEX/Poseidon sea surface height measurements, the comparisons shown in Figure 6 are for the time interval 1993–2001. Like the 50-year series, the 20-year and data assimilative OAM series were corrected for Boussinesq effects, were converted to equivalent polar motion excitation functions, and 10-day averages of their daily values were formed in order to make them consistent with the 50-year series.

[36] Power spectra and coherence magnitude and phase of the observed nonatmospheric polar motion excitation series and the three modeled oceanic excitation series are shown in Figure 6. Not surprisingly, the data assimilative oceanic excitation series (green curves) generally agrees best with the observed nonatmospheric excitation, especially at retrograde frequencies. The 50-year (red curves) and 20-year (blue curves) series show similar agreement with the observed nonatmospheric series except at seasonal frequencies where the 50-year series is in much better agreement with the observations than either the 20-year or even the data assimilative series. At frequencies of ±1 cpy, the 50-year series is in closest agreement with the observed nonatmospheric excitation series, showing the best agreement in both power and coherence. Thus the use of lopped cells, along with the slightly greater poleward extent of the model, greatly improves the accuracy of the modeled oceanic angular momentum at seasonal frequencies.

[37] Comparing results for the two simulations and the data assimilative series in Figure 6b shows that when data is used to constrain the model the greatest improvement in the coherence between the OAM and the observed nonatmospheric polar motion excitation functions occurs

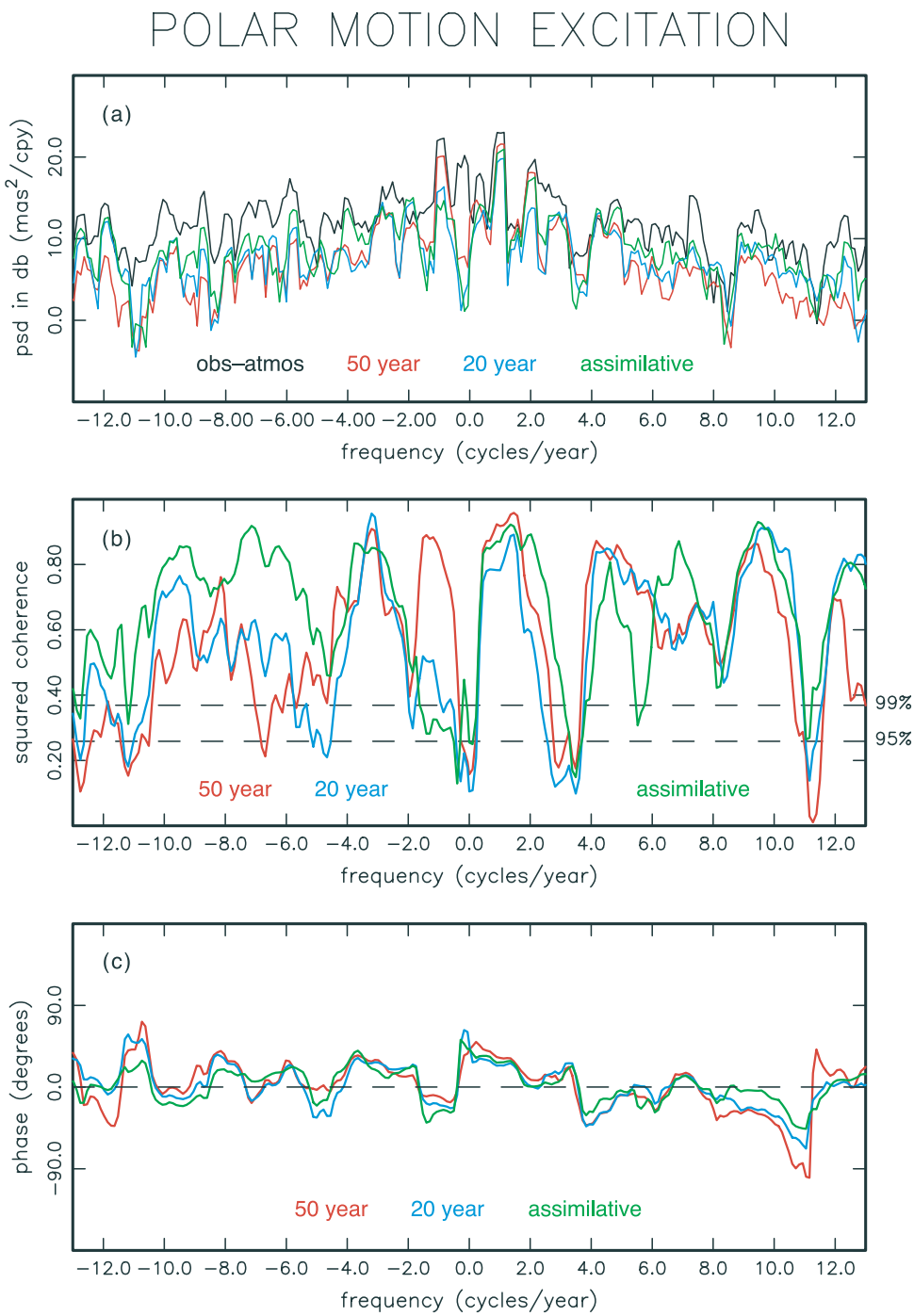

Figure 6. (a) Power spectral density (psd) estimates in decibels (dB) computed by the multitaper method of observed polar motion excitation variations during 1993–2001 from which the effects of atmospheric winds and surface pressure have been removed using the NCEP/NCAR reanalysis AAM series (black curve), the variations due to the 50-year oceanic excitation series (red curve), the 20-year oceanic excitation series (blue curve), and the data assimilative oceanic excitation series (green curve). (b) Squared magnitude of the coherence and (c) the phase, respectively, between the observed nonatmospheric polar motion excitation variations and the variations due to the 50-year (red curves), 20-year (blue curves), and data assimilative (green curves) oceanic excitation series. The retrograde component of polar motion excitation is represented by negative frequencies, the prograde component by positive frequencies. The horizontal dashed lines in Figure 6b indicate the 95% and 99% confidence levels of the magnitude of the squared coherence. Variations at the annual (1 cpy), semiannual (2 cpy), and terannual (3 cpy) frequencies have not been removed from the data sets prior to spectral and coherence estimation.

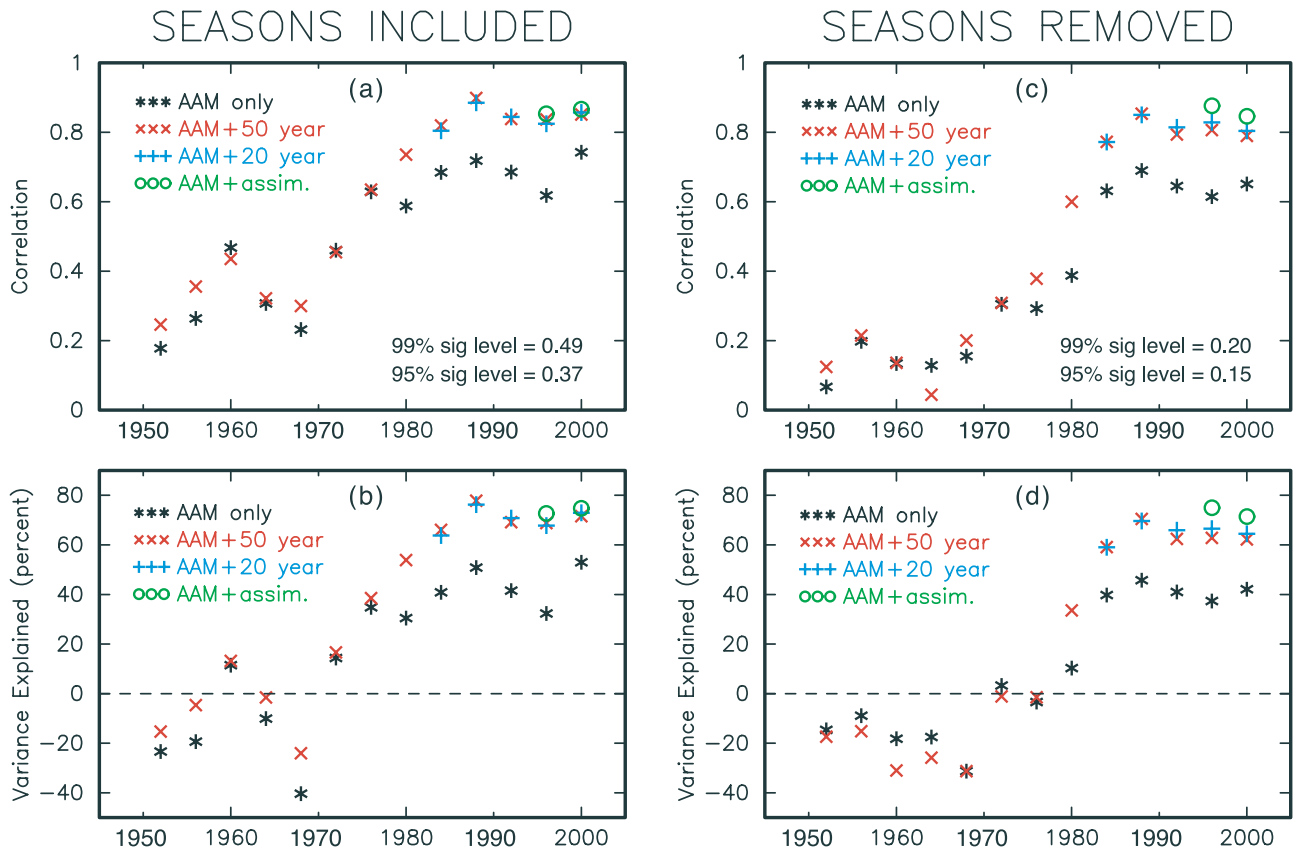

Figure 7. (a, c) Correlation between the observed and modeled polar motion excitation functions and (b, d) the percentage of the observed excitation variance explained by the modeled excitation in 4-year-long, nonoverlapping windows from 1950 through 2001 where the excitation functions are treated as being complex valued. A mean and trend has been computed and removed from the values within each window before computing the correlation and variance explained. In addition, the results shown in Figures 7c and 7d were obtained by also computing and removing a seasonal cycle from the values within each window. A negative variance explained in Figures 7b and 7d is obtained when the variance increases upon removing the modeled excitation from the observed. The AAM series (black asterisks) is the sum of the excitation due to winds and surface pressure where that due to the surface pressure has been computed by assuming that the oceans respond as an inverted barometer to the imposed pressure variations. The sum of the modeled atmospheric and the 50-year (red crosses), 20-year (blue pluses) and data assimilative (green circles) oceanic excitation series is the sum of the excitation due to winds, inverted barometer surface pressure, currents, and ocean bottom pressure.

at retrograde frequencies. In particular, the 20-year and 50-year simulation series have asymmetries in coherence with respect to prograde and retrograde frequencies, with the coherence at retrograde frequencies being noticeably lower than that at prograde frequencies. By comparison, the data assimilative series shows improved coherence at retrograde frequencies, so much so that similar coherence is achieved at retrograde and prograde frequencies.

5.3. Temporal Evolution of Excitation

[38] The accuracy of the observed polar motion excitation series used here improves with time as measurements from the more accurate space-geodetic techniques supplant the less accurate optical astrometric measurements. While the models of the atmospheric and oceanic analysis systems used here have been frozen, the accuracy of the modeled atmospheric and oceanic excitation series can also be expected to improve with time due to improvements in the accuracy, number, and type of measurements that are being assimilated into the models and, in the case of the oceanic excitation series, due to improvements in the accuracy of the atmospheric fields that are used to force the ocean model. This improvement in the accuracy of the observed and modeled polar motion excitation series can be expected to lead to improvements in the agreement between the series. The temporal evolution of the agreement between the observed and modeled polar motion excitation series is studied here by computing the correlation between the series and the percentage of the observed variance explained by the modeled series in 4-year-long, nonoverlapping windows from 1950 through 2001.

[39] As seen in Figure 7a, the correlation between the observed and the sum of atmospheric wind and inverted barometer pressure excitation series (black asterisks) becomes significant at the 99% level only after 1976.

Figure 7b shows that except for 1960, removing the modeled excitation from the observations reduces the variance only after 1972. Adding the sum of oceanic current and bottom pressure excitation to atmospheric wind and surface pressure excitation is seen to substantially improve both the correlation and the amount of the observed variance explained by the modeled series. The sum of the atmospheric and the 50-year (red crosses) and 20-year (blue pluses) oceanic excitation series show similar agreement with the observations, with the best agreement being obtained, as expected, with the sum of the atmospheric and the data assimilative oceanic excitation series (green circles).

[40] Similar results are obtained when the seasonal cycle is first removed from each 4-year-long window by least squares fitting and removing periodic signals with frequencies of 1 cpy, 2 cpy, and 3 cpy. Figure 7c shows that the correlation between the observed and modeled nonseasonal excitation becomes significant at the 99% level only after 1972, with Figure 7d showing that removing the modeled nonseasonal excitation from the observations reduces the variance only after 1980. Adding oceanic excitation to atmospheric substantially improves the agreement of the modeled nonseasonal excitation with the observations, with the best agreement again being obtained with the data assimilative oceanic series.

[41] The marked improvement shown in Figure 7 of the agreement between the observed and modeled polar motion excitation series starting in the mid to late 1970s is probably due to improvements in the accuracy of both the observed and modeled series. As discussed above, accurate polar motion measurements from the space-geodetic techniques became available in 1976, leading to more accurate polar motion excitation observations. In addition, the satellite era of global weather observing systems began in 1979 when global temperature soundings from satellites were first introduced [*Kistler et al.*, 2001]. This led to a substantial increase in atmospheric data coverage, particularly in the southern hemisphere, and thus to a substantial increase in the accuracy of the atmospheric fields that are used to both compute atmospheric angular momentum and to force the ocean model used to compute oceanic angular momentum. Improvements like these in both the observed and modeled excitation series have led to the remarkable level of agreement seen in Figure 7 between the observed and modeled polar motion excitation series since 1984, with correlations as great as 0.88 and with as much as 75% of the observed variance being explained by the sum of the modeled atmospheric and oceanic excitation.

6. Discussion and Summary

[42] Atmospheric and oceanic excitation of decadal-scale Earth orientation variations during 1949–2002 has been studied here using an atmospheric angular momentum series computed from the NCEP/NCAR reanalysis project and an oceanic angular momentum series computed from a near-global ocean model that was forced by surface fluxes from the NCEP/NCAR reanalysis project. As expected, the contribution of atmospheric and oceanic processes to exciting length-of-day variations on decadal timescales is minor, amounting to only 14% of the observed peak-to-peak variations during 1956–2002. More surprisingly, it has also been found that atmospheric and oceanic processes are unable to excite decadal polar motion variations to their observed level, amounting to only 20% (x component) and 38% (y component) of the observed peak-to-peak variations during 1949–2002, with the modeled and observed variations being 180° out of phase. This result indicates that redistribution of mass within the atmosphere and oceans cannot be the main excitation source of decadal polar motion variations.

[43] Interactions between the fluid outer core and mantle also appear to be ineffective in exciting decadal polar motion variations. Electromagnetic coupling between the core and mantle appears to be 2–3 orders of magnitude too weak [*Greff-Lefftz and Legros*, 1995] and topographic coupling appears to be too weak by a factor of three to ten [*Greff-Lefftz and Legros*, 1995; *Hide et al.*, 1996; *Hulot et al.*, 1996]. In addition, the modeled decadal polar motion variations resulting from these studies show little agreement in phase with the observed variations.

[44] However, *Dumberry and Bloxham* [2002] have recently shown that a tilt of the inner core with respect to the mantle of only 0.07°, perhaps caused by an electromagnetic torque acting on the inner core, would generate gravitational and pressure torques on the mantle strong enough to excite decadal polar motion variations having amplitudes as large as those observed and, like the observed variations, having a preferred direction of motion.

[45] Alternatively, nonsteric sea level height change due to glacier and ice sheet mass change may also be effective in exciting decadal polar motion variations. *Wilson* [1993] noted that an oscillation in global sea level on decadal timescales would excite decadal polar motion variations with a polarization similar to that observed, implying that mass change of the oceans is responsible for exciting the observed decadal polar motions. Here it has been shown that redistribution of mass within the oceans do not excite decadal polar motions to their observed level. However, the ocean model used in this study was not forced by mass changes associated with precipitation, evaporation, or runoff from rivers including that from glaciers and ice sheets, and hence has a constant total mass. So, this study does not address the question of the excitation of decadal polar motion by processes that change the total mass of the oceans, such as nonsteric sea level height change associated with glacier and ice sheet mass change. As mentioned earlier, using a climate model, *Celaya et al.* [1999] showed that changes in Antarctic snowpack are capable of inducing decadal polar motion variations of nearly the same amplitude as that observed. Realistic estimates of mass change in glaciers and the Antarctic and other ice sheets, along with estimates of the accompanying nonsteric change in sea level, are required to further evaluate this possible source of decadal polar motion excitation.

[46] **Acknowledgments.** We thank S. Dickman for his thorough review and an anonymous reviewer for additional comments that helped improve the paper. The work described in this paper was performed at the Jet Propulsion Laboratory, California Institute of Technology, under contract with the National Aeronautics and Space Administration. Support for

this work was provided by the Oceanography Program of NASA's Office of Earth Science. The supercomputer used in this investigation was provided by funding from JPL Institutional Computing and Information Services and the NASA Offices of Earth Science, Aeronautics, and Space Science. This is a contribution of the Consortium for Estimating the Circulation and Climate of the Ocean (ECCO) funded by the National Oceanographic Partnership Program.

References

Adcroft, A., C. Hill, and J. Marshall (1997), Representation of topography by shaved cells in a height coordinate ocean model, *Mon. Weather Rev.*, *125*, 2293–2315.

Barnes, R. T. H., R. Hide, A. A. White, and C. A. Wilson (1983), Atmospheric angular momentum fluctuations, length-of-day changes and polar motion, *Proc. R. Soc. London, Ser. A*, *387*, 31–73.

Brzezinski, A. (1992), Polar motion excitation by variations of the effective angular momentum function: Considerations concerning deconvolution problem, *Manuscr. Geod.*, *17*, 3–20.

Brzezinski, A., J. Nastula, and R. M. Ponte (2002), Oceanic excitation of the Chandler wobble using a 50-year time series of ocean angular momentum, in *Vistas for Geodesy in the New Millennium*, *IAG Symp.*, vol. 125, edited by J. Adám and K.-P. Schwarz, pp. 434–439, Springer, New York.

Brzezinski, A., J. Nastula, B. Kolaczek, and R. M. Ponte (2005), Oceanic excitation of polar motion from intraseasonal to decadal periods, in *A Window on the Future of Geodesy*, *IAG Symp.*, vol. 128, edited by F. Sanso, Springer, New York.

Carton, J. A., G. Chepurin, X. Cao, and B. Giese (2000), A simple ocean data assimilation analysis of the global upper ocean 1950-95. part I: Methodology, *J. Phys. Oceanogr.*, *30*(2), 294–309.

Celaya, M. A., J. M. Wahr, and F. O. Bryan (1999), Climate-driven polar motion, *J. Geophys. Res.*, *104*, 12,813–12,829.

Chao, B. F., R. D. Ray, J. M. Gipson, G. D. Egbert, and C. Ma (1996), Diurnal/semidiurnal polar motion excited by oceanic tidal angular momentum, *J. Geophys. Res.*, *101*, 20,151–20,163.

Conkright, M. E., et al. (1999), *World Ocean Database 1998*, *Internal Rep. 14*, Natl. Oceanogr. Data Cent., NOAA., Silver Spring, Md.

Defraigne, P., and I. Smits (1999), Length of day variations due to zonal tides for an inelastic earth in non-hydrostatic equilibrium, *Geophys. J. Int.*, *139*, 563–572.

de Viron, O., D. Salstein, C. Bizouard, and L. Fernandez (2004), Low-frequency excitation of length of day and polar motion by the atmosphere, *J. Geophys. Res.*, *109*, B03408, doi:10.1029/2003JB002817.

Dickman, S. R. (2003), Evaluation of "effective angular momentum function" formulations with respect to core-mantle coupling, *J. Geophys. Res.*, *108*(B3), 2150, doi:10.1029/2001JB001603.

Dumberry, M., and J. Bloxham (2002), Inner core tilt and polar motion, *Geophys. J. Int.*, *151*, 377–392.

Eubanks, T. M. (1993), Variations in the orientation of the Earth, in *Contributions of Space Geodesy to Geodynamics: Earth Dynamics*, *Geodyn. Ser.*, vol. 24, edited by D. E. Smith and D. L. Turcotte, pp. 1–54, AGU, Washington, D. C.

Gent, P. R., and J. C. McWilliams (1990), Isopycnal mixing in ocean circulation models, *J. Phys. Oceanogr.*, *20*, 150–160.

Greatbatch, R. J. (1994), A note on the representation of steric sea level in models that conserve volume rather than mass, *J. Geophys. Res.*, *99*, 12,767–12,771.

Greff-Lefftz, M., and H. Legros (1995), Core-mantle coupling and polar motion, *Phys. Earth Planet. Inter.*, *91*, 273–283.

Gross, R. S. (1992), Correspondence between theory and observations of polar motion, *Geophys. J. Int.*, *109*, 162–170.

Gross, R. S. (2003), Combinations of Earth orientation measurements: SPACE2002, COMB2002, and POLE2002, *JPL Publ.*, *03-011*, 28 pp.

Gross, R. S., and J. Vondrák (1999), Astrometric and space-geodetic observations of polar wander, *Geophys. Res. Lett.*, *26*, 2085–2088.

Gross, R. S., K. H. Hamdan, and D. H. Boggs (1996), Evidence for excitation of polar motion by fortnightly ocean tides, *Geophys. Res. Lett.*, *23*, 1809–1812.

Gross, R. S., B. F. Chao, and S. Desai (1997), Effect of long-period ocean tides on the Earth's polar motion, *Prog. Oceanogr.*, *40*, 385–397.

Gross, R. S., T. M. Eubanks, J. A. Steppe, A. P. Freedman, J. O. Dickey, and T. F. Runge (1998), A Kalman filter-based approach to combining independent Earth orientation series, *J. Geod.*, *72*, 215–235.

Gross, R. S., I. Fukumori, and D. Menemenlis (2003), Atmospheric and oceanic excitation of the Earth's wobbles during 1980–2000, *J. Geophys. Res.*, *108*(B8), 2370, doi:10.1029/2002JB002143.

Hide, R., D. H. Boggs, J. O. Dickey, D. Dong, R. S. Gross, and A. Jackson (1996), Topographic core-mantle coupling and polar motion on decadal time scales, *Geophys. J. Int.*, *125*, 599–607.

Hulot, G., M. Le Huy, and J.-L. Le Mouël (1996), Influence of core flows on the decade variations of the polar motion, *Geophys. Astrophys. Fluid Dyn.*, *82*, 35–67.

James, T. S., and E. R. Ivins (1997), Global geodetic signatures of the Antarctic ice sheet, *J. Geophys. Res.*, *102*, 605–633.

Kalnay, E., et al. (1996), The NCEP/NCAR 40-year reanalysis project, *Bull. Am. Meteorol. Soc.*, *77*, 437–471.

Kantha, L. H., J. S. Stewart, and S. D. Desai (1998), Long-period lunar fortnightly and monthly ocean tides, *J. Geophys. Res.*, *103*, 12,639–12,647.

Kistler, R., et al. (2001), The NCEP–NCAR 50-year reanalysis: Monthly means CD-ROM and documentation, *Bull. Am. Meteorol. Soc.*, *82*, 247–267.

Large, W. G., J. C. McWilliams, and S. C. Doney (1994), Oceanic vertical mixing: A review and a model with a nonlocal boundary layer parameterization, *Rev. Geophys.*, *32*, 363–403.

Large, W. G., G. Danabasoglu, S. C. Doney, and J. C. McWilliams (1997), Sensitivity to surface forcing and boundary layer mixing in a global ocean model: Annual-mean climatology, *J. Phys. Oceanogr.*, *27*, 2418–2447.

Li, Z., and M. Feissel (1986), Determination of the Earth rotation parameters from optical astrometry observations, 1962.0–1982.0, *Bull. Geod.*, *60*, 15–28.

Markowitz, W. (1960), Latitude and longitude, and the secular motion of the pole, in *Methods and Techniques in Geophysics*, edited by S. K. Runcorn, pp. 325–361, Wiley-Interscience, Hoboken, N. J.

Markowitz, W. (1961), International determination of the total motion of the pole, *Bull. Geod.*, *59*, 29–41.

Marshall, J., C. Hill, L. Perelman, and A. Adcroft (1997a), Hydrostatic, quasi-hydrostatic, and nonhydrostatic ocean modeling, *J. Geophys. Res.*, *102*, 5733–5752.

Marshall, J., A. Adcroft, C. Hill, L. Perelman, and C. Heisey (1997b), A finite-volume, incompressible, Navier Stokes model for studies of the ocean on parallel computers, *J. Geophys. Res.*, *102*, 5753–5766.

Menemenlis, D., I. Fukumori, and T. Lee (2005), Using Green's functions to calibrate an ocean general circulation model, *Mon. Weather Rev.*, *133*, 1224–1240.

Mitrovica, J. X., and G. A. Milne (1998), Glaciation-induced perturbations in the Earth's rotation: A new appraisal, *J. Geophys. Res.*, *103*, 985–1005.

Munk, W. H., and G. J. F. MacDonald (1960), *The Rotation of the Earth: A Geophysical Discussion*, 323 pp., Cambridge Univ. Press, New York.

Percival, D. B., and A. T. Walden (1993), *Spectral Analysis for Physical Applications: Multitaper and Conventional Univariate Techniques*, 610 pp., Cambridge Univ. Press, New York.

Ponsar, S., V. Dehant, R. Holme, D. Jault, A. Pais, and T. Van Hoolst (2003), The core and fluctuations in the Earth's Rotation, in *Earth's Core: Dynamics, Structure, Rotation*, *Geodyn. Ser.*, vol. 31, edited by V. Dehant et al., pp. 251–261, AGU, Washington, D. C.

Ponte, R. M., J. Rajamony, and J. M. Gregory (2002), Ocean angular momentum signals in a climate model and implications for Earth rotation, *Clim. Dyn.*, *19*, 181–190.

Redi, M. H. (1982), Oceanic isopycnal mixing by coordinate rotation, *J. Phys. Oceanogr.*, *12*, 1154–1158.

Rosen, R. D. (1993), The axial momentum balance of Earth and its fluid envelope, *Surv. Geophys.*, *14*, 1–29.

Salstein, D. A., and R. D. Rosen (1997), Global momentum and energy signals from reanalysis systems, paper presented at 7th Conference on Climate Variations, Am. Meteorol. Soc., Boston, Mass.

Salstein, D. A., D. M. Kann, A. J. Miller, and R. D. Rosen (1993), The Sub-Bureau for Atmospheric Angular Momentum of the International Earth Rotation Service: A meteorological data center with geodetic applications, *Bull. Am. Meteorol. Soc.*, *74*, 67–80.

Stammer, D., C. Wunsch, I. Fukumori, and J. Marshall (2002), State estimation improves prospects for ocean research, *Eos Trans. AGU*, *83*(27), 289, 294–295.

Stammer, D., K. Ueyoshi, A. Köhl, W. G. Large, S. A. Josey, and C. Wunsch (2004), Estimating air-sea fluxes of heat, freshwater, and momentum through global ocean data assimilation, *J. Geophys. Res.*, *109*, C05023, doi:10.1029/2003JC002082.

Steinberger, B. M., and R. J. O'Connell (1997), Changes of the Earth's rotation axis inferred from advection of mantle density heterogeneities, *Nature*, *387*, 169–173.

Trupin, A. S. (1993), Effects of polar ice on the Earth's rotation and gravitational potential, *Geophys. J. Int.*, *113*, 273–283.

Vermeersen, L. L. A., A. Fournier, and R. Sabadini (1997), Changes in rotation induced by Pleistocene ice masses with stratified analytical Earth models, *J. Geophys. Res.*, *102*, 27,689–27,702.

Vondrák, J., I. Pesek, C. Ron, and A. Cepek (1998), Earth orientation parameters 1899.7–1992.0 in the ICRS based on the Hipparcos reference frame, *Publ. 87*, 56 pp., Astron. Inst., Acad. of Sci. of the Czech Repub., Ondrejov, Czech Republic.

Wahr, J. M. (1982), The effects of the atmosphere and oceans on the Earth's wobble - I. Theory, *Geophys. J. R. Astron. Soc.*, *70*, 349–372.

Wilson, C. R. (1993), Contributions of water mass redistribution to polar motion excitation, in *Contributions of Space Geodesy to Geodynamics: Earth Dynamics*, *Geodyn. Ser.*, vol. 24, edited by D. E. Smith and D. L. Turcotte, pp. 77–82, AGU, Washington, D. C.

Wunsch, C., and D. Stammer (1997), Atmospheric loading and the oceanic "inverted barometer" effect, *Rev. Geophys.*, *35*, 79–107.

Yoder, C. F., J. G. Williams, and M. E. Parke (1981), Tidal variations of Earth rotation, *J. Geophys. Res.*, *86*, 881–891.

I. Fukumori, R. S. Gross, and D. Menemenlis, Jet Propulsion Laboratory, California Institute of Technology, 4800 Oak Grove Drive, Mail Stop 238-600, Pasadena, CA 91109-8099, USA. (richard.gross@jpl.nasa.gov)